Article ID: 1000-324X(2017)02-0219-06 **DOI:**10.15541/jim20160280

Colossal Permittivity and Dielectric Relaxations of (Nb, Al) Co-doped $BaTiO_3$ Ceramics

HUANG Dong[1, 2], WU Ying[1], MIAO Ji-Yuan[1], LIU Zhi-Fu[1], LI Yong-Xiang[1]

(1. CAS Key Lab of Inorganic Functional Materials and Devices, Shanghai Institute of Ceramics, Chinese Academy of Sciences, Shanghai 200050, China; 2. School of Physical Science and Technology, Shanghai Tech University, Shanghai 201210, China)

Abstract: Nb and Al co-doped $BaTiO_3$ ceramics, $BaTi_{0.98}(Nb_{0.5}Al_{0.5})_{0.02}O_3$, have a colossal permittivity ($\varepsilon_r \approx 3\times10^5$, $\tan\delta \approx 0.2$) at room-temperature. Three distinct relaxation processes are observed in the frequency range from 10^{-1} to 10^7 Hz. The low-frequency relaxation between 10^{-1} and 10 Hz and the intermediate-frequency relaxation between 10^3 and 10^5 Hz are non-Debye relaxations, which are attributed to Maxwell-Wagner interfacial polarization, electrode interfacial polarization, and barrier layer capacitor. While the high-frequency process between 10^5 and 10^7 Hz is a typical Debye-type relaxation with an activation energy of $E \approx 15$ meV and a frequency factor of $f_0 \approx 7\times10^6$ Hz. The small activation energy and relatively small frequency factor in the $BaTi_{0.98}(Nb_{0.5}Al_{0.5})_{0.02}O_3$ ceramics indicate that this relaxation process may derive from local motion of electrons in the complex defect clusters, which results from co-doping and can be named as electron-pinned defect-dipoles. This study suggests that the electron-pinned defect-dipoles mechanism can be used to design colossal permittivity in perovskites, like $BaTiO_3$.

Key words: (Nb, Al) co-doped; perovskites; colossal permittivity; electron-pinned defect-dipoles

Dielectrics with colossal permittivity (CP, $\varepsilon_r > 10^3$) have been recently drawn immense research attention due to their potential application in multilayer ceramic capacitors (MLCC) and energy storage[1-4]. Generally, CP in traditional dielectrics, originating from barrier layer capacitor (BLC) effect[5], charge-density wave (CDW)[6] and ferroelectricity[7], suffers from either high dielectric loss or poor temperature stability. To meet the high standards, including colossal permittivity, excellent frequency-stability, temperature-stability and low dielectric loss are still challenges.

Recently, a strategy, named the electron-pinned defect-dipoles mechanism, has been proposed to design CP in dielectrics[8]. Through donor and acceptor heteroatomic substitutions, carriers injected by doping can be confined by the local lattice defect clusters (about few metal-oxygen polyhedral) and contribute to the formation of the electron-pinned defect dipoles. Compared to atomic electrons, these electrons within the lattice defect clusters, have more considerable space for displacement under external electric field. Then the resultant large defect dipoles lead to an experimentally observed CP of ~ 6×10^4 in the (Nb, In) co-doped TiO_2 ceramics. Meanwhile, due to the localization of carriers, low dielectric loss, good temperature and frequency stability are also achieved. Electron-pinned defect-dipoles were first reported in (Nb, In) co-doped TiO_2. However, it is an interesting question not only for fundamental research but also for practical applications that whether such electron-pinned defect-dipoles can be achieved in other materials.

In electron-pinned defect-dipoles, the correlation among defects is crucial for forming defect clusters to localize carries. This kind of interaction between lattice defects and carriers has also been reported in perovskites such as $BaTiO_3$ and $SrTiO_3$[9-10]. In Nb-doped $BaTiO_3$ crystal, electrons can be trapped by Nb impurities so that local polar clusters are formed. In return, the electron relaxation in the polarized clusters improves the relaxation step (ε_s–ε_∞) by 25 times comparing to pure $BaTiO_3$[9]. In $SrTiO_3$, electrons can be localized in the defect clusters, $V_O^{\bullet\bullet} - Ti^{3+}$, exhibiting behaviors of small polaron and blue luminescence[10]. These results indicate that electron-pinned defect-dipoles could be realized in perovskites if the lattice defects or defect pairs are carefully modulated. Therefore, in present work, the dielectric properties and relaxation mechanisms of (Nb, Al) co-doped $BaTiO_3$ ce-

Received date: 2016-04-25; **Modified date:** 2016-06-06
Foundation item: National Natural Science Foundation of China (51572279); 973 Program (2015CB654604, 2015CB654605); International Science and Technology Cooperation Program of China (2015DFA51100)
Biography: HUANG Dong (1992–), male, candidate of Master degree. E-mail: donghuang9245@foxmail.com
Corresponding author: LI Yong-Xiang, professor. E-mail: yxli@mail.sic.ac.cn; LIU Zhi-Fu, professor. E-mail: liuzf@mail.sic.ac.cn

ramics are investigated. And a relaxation peak, related to the electron-pinned defects dipoles, emerges in the high frequency range between 10^6 and 10^7 Hz.

1 Experimental

Appropriate amount of raw materials, $BaCO_3$ (≥99.95%), TiO_2 (≥99.99%), Nb_2O_5 (≥99.99%) and Al_2O_3 (≥99.99%, all from Aladdin, China), according to the formula of $BaTi_{0.98}(Nb_{0.5}Al_{0.5})_{0.02}O_3$ (BTNA) was well mixed, pre-sintered at 1423 K for 4 h. Then the pre-sintered powders were re-milled and pressed at 200 MPa by cold isostatic pressing into discs (13 mm in diameter and about 1.5 mm in thickness). After burning off the binder, samples were sintered at 1593 K in air for 6 h. Post-annealing in oxygen for 12 h at 1473 K was adopted to compensate the loss of oxygen during high temperature sintering.

The crystal structures of samples were investigated using X-ray diffraction with Cu-Kα radiation (Rigaku D/MAX-2550 X-ray diffractometer, Japan). Microstructures of sintered ceramics were observed on the thermally etched polished-surface with scanning electron microscopy (SEM, Supra 55, Carl Zeiss, Germany). Dielectric properties were measured using a Broadband Dielectric Spectrometer (Novocontrol, Concept 40, Germany). X-ray photoelectron spectroscopy (XPS) was performed on the ceramic fresh fracture with a VG Escalab 250 apparatus for Ti oxidation states determination.

2 Results and discussion

Fig. 1 shows the temperature dependence of dielectric spectra of BTNA and pure $BaTiO_3$ ceramics. Comparing to $BaTiO_3$, the permittivity of BTNA is significantly improved. Colossal permittivity, $\varepsilon_r > 10^5$, is observed for BTNA ceramic sample between 150 K and 450 K. Meanwhile, the temperature stability of BTNA is also enhanced. There is no permittivity peak related to the phase transition which is observed in the $BaTiO_3$ sample. The permittivity shows a relatively flat platform at the temperature range from 280 K to 370 K. The considerable improvement of permittivity and its temperature stability in BTNA demonstrates that its CP doesn't originate from ferroelectricity. No impurity phase is found in XRD pattern and the shift of the diffraction peaks implies that Nb and Al have been introduced into the lattice of the $BaTiO_3$ crystal grains. The microstructural and elemental investigation also show the uniform distribution of dopants. And the BTNA ceramic is single tetragonal phase, the same as $BaTiO_3$[11]. Hence, the CP should not be from other phases.

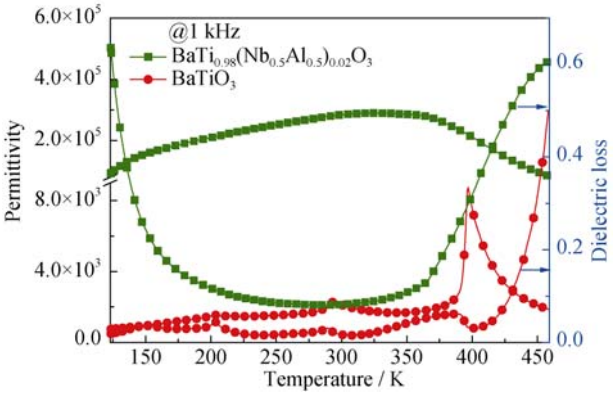

Fig. 1 Temperature dependence of permittivity and dielectric loss for $BaTiO_3$ ceramic sintered at 1623 K/6 h and BTNA ceramic sintered at 1593 K/6 h in temperature range from 123 K to 459 K

To identify the characteristics of the dielectric properties of BTNA ceramic, room-temperature frequency dependence of the dielectric permittivity and loss tangent of BTNA were measured as shown in Fig. 2. The frequency dependences of dielectric properties of several typical dielectrics are presented in Fig. 2 as well[8, 12-14]. BTNA shows a high permittivity, $\varepsilon_r > 3\times10^5$ in the low frequency range ($f<10^3$ Hz). As the frequency increases, the permittivity decreases gradually and two permittivity steps, including intermediate-frequency step in the frequency range between 10^3 and 10^5 Hz and high-frequency step in the range between 10^5 and 10^7 Hz, are clearly seen. Meanwhile, two corresponding dielectric loss peaks, Peak 1 and Peak 2, in the same frequency range are observed. The two-step character of the dielectric properties in BTNA is significantly different from the frequency dependence of CP deriving from BLC effect in (Li, Ti) co-doped NiO and SPS sintered $BaTiO_3$ ceramics, where only one permittivity step and one loss peak in the intermediate frequency range are observed. For $CaCu_3Ti_4O_{12}$, though the origin of its CP is still controversial, there is also only one permittivity step. For (Nb, In) co-doped TiO_2, the permittivity does not show a step when the frequency is below 10^6 Hz. But the gradual increase of the dielectric loss with increasing of the test frequency indicates that there may be a loss peak in the higher frequency range ($f>10^6$ Hz). The unique frequency dependence of the permittivity and dielectric loss of BTNA means that the CP in BTNA cannot be explained by either barrier layer capacitor effect or electron-pinned defect-dipoles alone. The two-step character indicates that there should be at least two polarization mechanisms contributing to the CP in BTNA. The consistence of the intermediate-frequency step and dielectric loss peak between BTNA and (Li, Ti) co-doped NiO or SPS sintered $BaTiO_3$ reveals that this step may be related to the BLC effect.

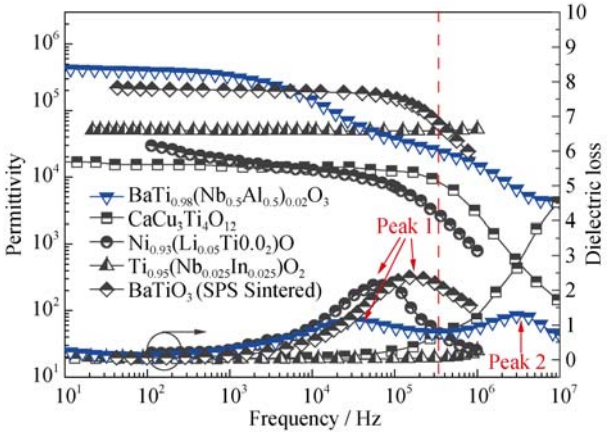

Fig. 2 Comparison of the dependent permittivity and dielectric loss of BTNA, $CaCu_3Ti_4O_{12}$[12], (Li, Ti) co-doped NiO[14], (Nb, In) co-doped TiO_2[8] and spark plasma sintered $BaTiO_3$[13] in the frequency range from 10 Hz to 10^7 Hz

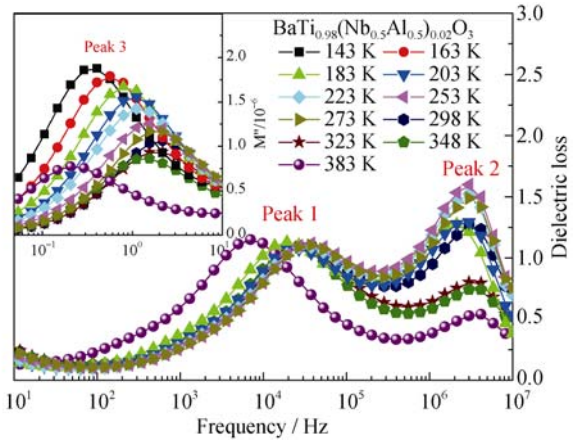

Fig. 3　Frequency dependence of the dielectric loss of BTNA ceramic in the frequency range from 10 Hz to 10^7 Hz measured from 143 K to 383 K. The inset shows the M'' spectroscopic plots for the BTNA at low frequency range (0.04 Hz to 10 Hz)

To further depict the dielectric behavior of BTNA, the frequency dielectric spectrums of BTNA at various temperatures from 143 K to 383 K are shown in Fig. 3. In the frequency range between 10 Hz and 10^7 Hz, two dielectric loss peaks, Peak 1 and 2 can be identified. However, from the spectroscopic plot of the imaginary components of electric modulus, M'', another relaxation peak, named as Peak 3, is detected in the frequency range from 0.1 Hz to 10 Hz. Three peaks, including low-frequency Peak 3, intermediate-frequency Peak 1 and high-frequency Peak 2, shift as the temperature changes. The peak frequencies as functions of temperature are shown in Fig. 4. The intermediate-frequency Peak 1 and low-frequency Peak 3 show a similar shift trend as the temperature increases. At low temperature, the relaxation peaks shift to higher frequency as the temperature increases. While in the high temperature range (T>298 K for Peak 3, and T>253 K for Peak 1), this trend is surprisingly inversed and the peaks shift to lower frequency as the temperature increases. The similar behavior of Peak 1 and Peak 3 indicate that these two relaxation peaks should derive from a similar polarization mechanism. And this mechanism cannot be described by Debye model because the thermally activated behavior of the peak frequency is deviated.

As mentioned above, the intermediate-frequency Peak 1 may be ascribed to the BLC effect considering the similarities of this peak and the corresponding permittivity step to the results of typical BLC effect. While for the low-frequency Peak 3, such a slow response to the external electric field (relaxation time, $\tau = 1/2\pi f > 1$ s) indicates that this peak should originate from interfacial polarization[15]. It's well accepted that, in the relatively low frequency range below 10 Hz, interfaces between metallic electrodes and dielectrics have a significant influence on the dielectric properties and lead to a relaxation[16-18].

Either BLC effect or electrode interfacial polarization can be described by the Maxwell-Wagner (MW) interfacial polarization which arises from the electrical properties inhomogeneity in the ceramics. The general model for describing an inhomogeneous structure consists of double layers, which are characterized by its permittivity ε_1, ε_2, its conductivity σ_1, σ_2 and its thickness d_1, d_2[19]. The relaxation time then is

$$\tau = 1/2\pi f = \varepsilon_0 \frac{d_1\varepsilon_2 + d_2\varepsilon_1}{d_1\sigma_2 + d_2\sigma_1} \quad (1)$$

From Eq. (1) we can see that the relaxation time τ is dependent on the permittivity, ε and the conductivity, σ. Generally, both permittivity and conductivity are functions of temperature especially in $BaTiO_3$-based materials, where the series of phase transitions[20] and the positive temperature coefficient of resistivity (PTCR)[21] make the behavior of permittivity, ε_i and conductivity, σ even more complex as the temperature changes. The non-monotonic behavior of the relaxation time of MW polarization with the temperature increasing could be expected, which may be able to explain the distinct shift of Peak 1 and 3. Of course, further investigations are still in need to explain this phenomenon.

The behavior of Peak 2 in the high frequency range is clearly different from those of Peak 1 and Peak 3. The frequency of Peak 2 shifts to high frequency range monotonously as the temperature increases. The thermally activated behavior can be depicted by the Debye model with the characteristic relaxation frequency

$$f = f_0 \exp(-E/k_bT) \quad (2)$$

Where f_0, k_b and E are the pre-exponential frequency factor, Boltzmann constant and activation energy, respectively. Fig. 4 shows that the linear relationship of ln(f) to $1/T$ can

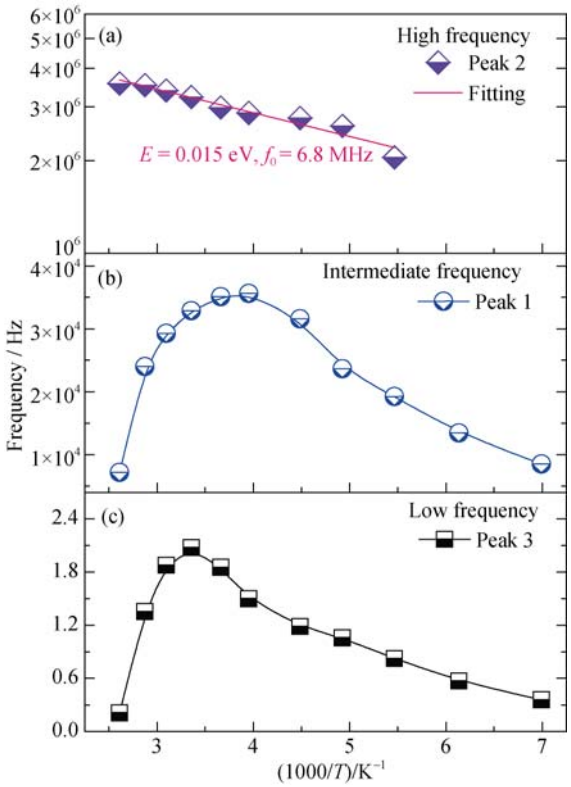

Fig. 4 The dependence of dielectric loss peak frequency on testing temperature from 143 K to 383 K

(a) Low frequency range (Peak 2); (b) Intermediate frequency range (Peak 1); (c) High frequency range (Peak 3)

fit the shift of Peak 2 very well. The pre-exponential factor f_0 is 6.8×10^6 Hz and the activation energy is only about 15 meV.

Small values of the activation energy mean that the relaxation peak should not derive from the motion of ions because its activation energy is in an order of 1 eV[22]. The relaxation should be ascribed to the movement of electrons. Carrier electrons are introduced into the lattice by substituting Nb^{5+} at Ti^{4+} sites. However, the order of frequency, at which the dielectric effects of free charge carriers become significant, is the reciprocal collision time, $f\approx10^{16}$ Hz[23], which is much higher than the testing frequency. So the movement of neither ions nor free electrons can be concluded to contribute to the observed high-frequency relaxation process. Nevertheless, the dielectric responses can also result from localized charge carriers. According to Anderson localization model[24], carriers can be localized by the disorder such as structural or compositional defects in the solid. The interaction between lattice defects and electrons can increase the effective mass of electrons and lead to a slower response to the external electric field or smaller frequency factor, f_0[23]. This may explain the small activation energy about 15 meV and relatively slow dielectric response with $f_0\approx10^7$ Hz.

According to the defect chemistry, lattice defects can interact with each other and form local defect clusters. The electrons can be pinned by the local defect clusters and respond to external electric field. It has been reported that, the electrons can be confined in the defect clusters, $Nb_{Ti}^{5+}Ti_{Ti}^{3+}$, and contribute to the Debye-type dielectric relaxation with the activation energy $E\approx10-20$ meV and relaxation time $\tau_0\approx10^8-10^{10}$ s^{-1} in $(1-x)SrTiO_3$ - $xSr(Mg_{1/3}Nb_{2/3})O_3$ ceramics[25]. In the (Nb, In) co-doped TiO_2 ceramics, the electrons hop within the local defect clusters, $Nb_2^{5+}Ti^{3+}A_{Ti}$ ($A=Ti^{3+},In^{3+},Ti^{4+}$) forming defect dipoles, the activation energy of which is about 15 meV[8]. In the reduced TiO_{2-x} crystal, the electrons hop within the complex ionic defect cores, which consist of normal Ti sites and trivalent or pentavalent impurities defects. And in that way, it causes the relaxation processes, which possess the activation energy of $E\approx1-20$ meV and the relaxation time of $\tau_0\approx10^6-10^8$ s^{-1}[26]. The activation energy and pre-exponential factor of Peak 2 are obviously close to the observations in these materials. Therefore, the high frequency relaxation peak might be derived from the electron hoping within the defect clusters.

To further explore the defect clusters in BTNA, the X-ray photoelectron spectroscopy (XPS) data of the fresh fracture was collected as shown in Fig. 5. The O1s spectrum in Fig. 5(a) exhibits two well-developed peaks. The peak at 529.3 eV corresponds to the lattice oxygen while the peak with the binding energy of 531.6 eV is associated with oxygen vacancies[27-29]. The peak at 531.6 eV is much higher than that of the pure $BaTiO_3$, which means the abundant oxygen vacancies in BTNA even though the sample has been post-annealed in oxygen at 1473 K for 12 h[29].

It is well established that the donor doping (*e.g.* Nb^{5+}) cannot induce oxygen vacancies while the acceptor doping (*e.g.* Al^{3+}) requires oxygen vacancies in terms of charge compensation as follows[30]:

$$2BaTiO_3+Al_2O_3\rightarrow2Ba_{Ba}^{\times}+2Al_{Ti}'+5O_O^{\times}+V_O^{\bullet\bullet} \quad (3)$$

The position of Ti2p doublet with $2p_{3/2}$ and $2p_{1/2}$ binding energy of 458.1 eV and 463.9 eV, respectively, is clearly presented in Fig. 5(b), corresponding to that of pure $BaTiO_3$[29]. In addition, noticeable Ti^{3+} peaks at 456.8 eV and 462.1 eV are also detected. The Ti^{3+} signals result from the reduction of Ti^{4+} by introduction of Nb^{5+} as follows[31-33]:

$$4BaTiO_3+2Nb_2O_5\rightarrow4Ba_{Ba}^{\times}+4Nb_{Ti}^{\bullet}+12O_O^{\times}+O_2\uparrow+4e' \quad (4)$$

$$Ti_{Ti}^{\times}+e'\rightarrow Ti_{Ti}' \quad (5)$$

The various defects such as $Nb_{Ti}^{\bullet}$, Al_{Ti}', Ti_{Ti}' and $V_O^{\bullet\bullet}$ co-exist in BTNA sample, interacting with each other to maintain the charge balance. As a result, the oxygen vacancies, $V_O^{\bullet\bullet}$, holding two positive charges, can connect to the

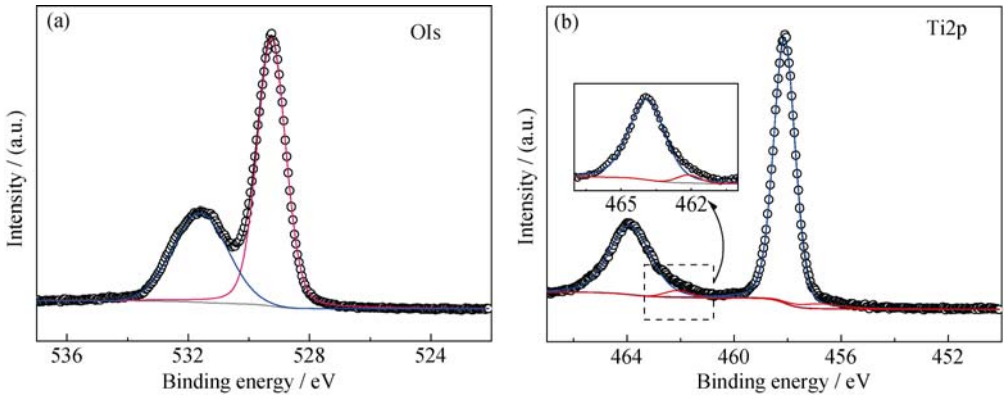

Fig. 5　Core level XPS (open circles) and corresponding fitting results (solids lines) of BTNA sample

nearest Al'_{Ti} or Ti'_{Ti} forming the defect clusters like $Al^{3+}_{Ti}V_O Ti_{Ti}$, $Ti^{3+}_{Ti}V_O Ti_{Ti}$, $Al^{3+}_{Ti}V_O Al_{Ti}$. Meanwhile, the $Nb^{\bullet}_{Ti}$ with one positive charge can also connect to the negative charge defects, Al'_{Ti} or Ti'_{Ti} forming $Nb^{\bullet}_{Ti}Al'_{Ti}$ and $Nb^{\bullet}_{Ti}Ti'_{Ti}$ clusters. Under these circumstances, the positive charge lattice defects $Nb^{\bullet}_{Ti}$ and $V^{\bullet\bullet}_{O}$ can all be correlated to Al'_{Ti} or Ti'_{Ti}. These defect clusters, for instance $Al^{3+}_{Ti}V_O Ti_{Ti}$, $Ti^{3+}_{Ti}V_O Ti_{Ti}$, $Al^{3+}_{Ti}V_O Al_{Ti}{}^{\bullet}$, $Nb^{\bullet}_{Ti}Al'_{Ti}$ and $Nb^{\bullet}_{Ti}Ti'_{Ti}$ can correlate or overlap together further, leading to larger complex defect clusters[8, 34]. In these defect clusters, the electrons are highly localized and limited to hop among lattice sites within the zones of the defect clusters. Under external electrical field, the pinned electrons in the defect clusters orientate forming the electron-pinned defect dipoles and giving rise to the high-frequency dielectric response observed in BTNA ceramics.

3　Conclusions

Colossal permittivity has been observed in the $Ba(Ti_{0.98}(Nb_{0.5}Al_{0.5})_{0.02}O_3$ ceramics with $\varepsilon_r \approx 3\times10^5$, $\tan\delta \approx 0.2$ at room temperature, 1 kHz. Three relaxation processes have been identified in the ceramics, which are electrode interfacial polarization at low-frequency, barrier layer capacitor effect at intermediate-frequency, and electron-pinned defect-dipoles polarization at high-frequency. The electron-pinned defect-dipoles polarization is firstly reported in $BaTiO_3$ ceramics which may open up more opportunities for us to design the colossal permittivity in ABO_3 perovskites.

References:

[1] LUNKENHEIMER P, KROHNS S, RIEGG S, *et al*. Colossal dielectric constants in transition-metal oxides. *The European Physical Journal Special Topics*, 2010, **180(1):** 61–89.

[2] KROHNS S, LUNKENHEIMER P, MEISSNER S, *et al*. The route to resource-efficient novel materials. *Nature Materials*, 2011, **10(12):** 899–901.

[3] HOMES C C, VOGT T, SHAPIRO S M, *et al*. Optical response of high-dielectric-constant perovskite-related oxide. *Science*, 2001, **293(5530):** 673–676.

[4] LI Y X. Some hot topics in electroceramics research. *Journal of Inorganic Materials*, 2014, **29(1):** 1–5.

[5] SARKAR S, JANA P K, CHAUDHURI B. Colossal internal barrier layer capacitance effect in polycrystalline copper (II) oxide. *Applied Physics Letters*, 2008, **92(2):** 022905–1–3.

[6] CAVA R J, FLEMING R M, LITTLEWOOD P, *et al*. Dielectric response of the charge-density wave in $K_{0.3}MoO_3$. *Physical Review B*, 1984, **30(6):** 3228–3239.

[7] IKEDA N, OHSUMI H, OHWADA K, *et al*. Ferroelectricity from iron valence ordering in the charge-frustrated system $LuFe_2O_4$. *Nature*, 2005, **436(7054):** 1136–1138.

[8] HU W B, LIU Y, WITHERS R L, *et al*. Electron-pinned defect-dipoles for high-performance colossal permittivity materials. *Nature Materials*, 2013, **12(9):** 821–826.

[9] MAGLIONE M, BELKAOUMI M. Electron relaxation-mode interaction in $BaTiO_3$-Nb. *Physical Review B*, 1992, **45(5):** 2029–2034.

[10] JANOTTI A, VARLEY J B, CHOI M, *et al*. Vacancies and small polarons in $SrTiO_3$. *Physical Review B*, 2014, **90(8):** 085202–1–3.

[11] BEN L B, SINCLAIR D C. Anomalous curie temperature behavior of A-site Gd-doped $BaTiO_3$ ceramics: the influence of strain. *Applied Physics Letters*, 2011, **98(9):** 092207–1–3.

[12] PATTERSON E A, KWON S, HUANG C C, *et al*. Effects of ZrO_2 additions on the dielectric properties of $CaCu_3Ti_4O_{12}$. *Applied Physics Letters*, 2005, **87(18):** 182911–1–3.

[13] HAN H, VOISIN C, GUILLEMET-FRITSCH S, *et al*. Origin of colossal permittivity in $BaTiO_3$ *via* broadband dielectric spectroscopy. *Journal of Applied Physics*. 2013, **113(2):** 024102–1–3.

[14] WU J, NAN C W, LIN Y, *et al*. Giant dielectric permittivity observed in Li and Ti doped NiO. *Physical Review Letters*, 2002, **89(21):** 217601–1–3.

[15] JONSCHER A K. Dielectric relaxation in solids. *Journal of*

Physics D: Applied Physics, 1999, **32(14):** R57–1–3.

[16] KROHNS S, LUNKENHEIMER P, KANT C, *et al*. Colossal dielectric constant up to gigahertz at room temperature. *Applied Physics Letters*, 2009, **94(12):** 122903–1–3.

[17] WANG H, LI G, ZHAO M, *et al*. Spin state transition and giant dielectric constant in $Pr_{0.987}Na_{0.013}CoO_3$. *Applied Physics Letters*, 2012, **100(15):** 152109–1–3.

[18] LI X, XU L, LIU L, *et al*. High pressure treated ZnO ceramics towards giant dielectric constants. *Journal of Materials Chemistry A*, 2014, **2(39):** 16740–16745.

[19] WAGNER K W. The theory of incomplete dielectricity. *Annalen Der Physik*, 1913, **40(5):** 817–855.

[20] KOLODIAZHNYI T, TACHIBANA M, KAWAJI H, *et al*. Persistence of ferroelectricity in $BaTiO_3$ through the insulator-metal transition. *Physical Review Letters*, 2010, **104(14):** 147602-1–3.

[21] KATAOKA N, HAYASHI K, YAMAMOTO T, *et al*. Direct observation of the double Schottky barrier in niobium-doped barium titanate by the charge-collection current method. *Journal of American Ceramics Society*, 1998, **81(7):** 1961–1963.

[22] BIDAULT O, GOUX P, KCHIKECH M, *et al*. Space-charge relaxation in perovskites. *Physical Review B*, 1994, **49(12):** 7868–7873.

[23] BIDAULT O, MAGLIONE M, ACTIS M, *et al*. Polaronic relaxation in perovskites. *Physical Review B*, 1995, **52(6):** 4191–4197.

[24] ANDERSON P W. Absence of diffusion in certain random lattices. *Physical Review*, 1958, **109(5):** 1492–1505.

[25] LEMANOV V V, SOTNIKOV A V, SMIRNOVA E P, *et al*. Giant dielectric relaxation in $SrTiO_3$-$SrMg_{1/3}Nb_{2/3}O_3$ and $SrTiO_3$-$SrSc_{1/2}Ta_{1/2}O_3$ solid solutions. *Physics of the Solid State*, 2002, **44(11):** 2039–2049.

[26] DOMINIK L A K, MACCRONE R K. Dielectric relaxations in reduced rutile TiO_{2-x} at low temperatures. *Physical Review*, 1967, **163(3):** 756.

[27] RAMOS-MOORE E, FERRARI P, DIAZ-DROGUETT D E, *et al*. Raman and X-ray photoelectron spectroscopy study of ferroelectric switching in $Pb(Nb,Zr,Ti)O_3$ thin films. *Journal of Applied Physics*, 2012, **111(1):** 014108–1–3.

[28] SHUAI Y, ZHOU S, BUERGER D, *et al*. Decisive role of oxygen vacancy in ferroelectric versus ferromagnetic Mn-doped $BaTiO_3$ thin films. *Journal of Applied Physics*, 2011, **109(8):** 084105–1–3.

[29] NASSER S A. X-ray photoelectron spectroscopy study on the composition and structure of $BaTiO_3$ thin films deposited on silicon. *Applied Surface Science*, 2000, **157(1/2):** 14–22.

[30] CHAN N H, SHARMA R, SMYTH D M. Nonstoichiometry in acceptor‐doped $BaTiO_3$. *Journal of American Ceramics Society*, 1982, **65(3):** 167–170.

[31] YANG N H, TSENG C C, WU J L, *et al*. One-step molten-salt synthesis of $BaTi_4O_9$ nanowires with oxygen deficiency-enhanced dielectric performance. *RSC Advances*, 2013, **3(19):** 7093–7099.

[32] LI W, ZHAO R, WANG L, *et al*. Oxygen-vacancy- induced antiferromagnetism to ferromagnetism transformation in $Eu_{0.5}Ba_{0.5}TiO_{3-\delta}$ multiferroic thin films. *Scientific Reports*, 2013, **3:** 2618.

[33] CHAN N H, SMYTH D M. Defect chemistry of donor‐doped $BaTiO_3$. *Journal of American Ceramics Society*, 1984, **67(4):** 285–288.

[34] GAI Z, CHENG Z, WANG X, *et al*. A colossal dielectric constant of an amorphous TiO_2:(Nb, In) film with low loss fabrication at room temperature. *Journal of Materials Chemistry C*, 2014, **2(33):** 6790–6795.

(Nb, Al)共掺 $BaTiO_3$ 陶瓷的巨介电及介电弛豫现象

黄 栋[1,2], 吴 颖[1], 苗纪远[1], 刘志甫[1], 李永祥[1]

(1. 中国科学院 上海硅酸盐研究所, 无机功能材料与器件重点实验室, 上海 200050; 2. 上海科技大学 物质科学与技术学院, 上海 201210)

摘 要: (Nb, Al)共掺的 $BaTiO_3$ 陶瓷($BaTi_{0.98}(Nb_{0.5}Al_{0.5})_{0.02}O_3$)表现出巨介电现象, 介电常数可以达到 3×10^5, 介电损耗为 0.2。在 10^{-1}~10^7 Hz 范围内, 观察到三种介电弛豫现象, 并分别对其进行了分析。低频段(10^{-1}~10 Hz)和中频段(10^3~10^5 Hz)属于非德拜弛豫, 分别是由于 Maxwell-Wagner 电极界面极化和晶界层电容器效应引起的; 相反, 高频段(10^5~10^7 Hz)属于德拜弛豫, 通过阿伦尼乌斯公式的拟合, 得到其激活能 $E = 15$ meV 和频率因子 $f_0 = 7\times10^6$ Hz。较小的激活能和频率因子表明其弛豫过程可能来源于复杂缺陷团簇中的电子的局域运动, 被称为钉扎电子‐缺陷偶极子效应。本研究显示钉扎电子‐缺陷偶极子效应可以作为设计新型巨介电钙钛矿材料的依据。

关 键 词: (Nb, Al)共掺; 钙钛矿; 巨介电常数; 钉扎电子–缺陷偶极子

中图分类号: TQ174 **文献标识码:** A